DOI: 10.1002/chem.200700727

The Rate-Determining Step in the Rhodium–Xantphos-Catalysed Hydroformylation of 1-Octene

Erik Zuidema,[a] Laura Escorihuela,[b] Tanja Eichelsheim,[a] Jorge J. Carbó,[b] Carles Bo,[b, c] Paul C. J. Kamer,[a] and Piet W. N. M. van Leeuwen*[a, c]

Abstract: The rate-determining step in the hydroformylation of 1-octene, catalysed by the rhodium–Xantphos catalyst system, was determined by using a combination of experimentally determined $^{1}H/^{2}H$ and $^{12}C/^{13}C$ kinetic isotope effects and a theoretical approach. From the rates of hydroformylation and deuterioformylation, a small $^{1}H/^{2}H$ isotope effect of 1.2 was determined for the hydride moiety of the rhodium catalyst. $^{12}C/^{13}C$ isotope effects of 1.012(1) and 1.012(3) for the α-carbon and β-carbon atoms of 1-octene were determined, respectively. Both quantum mechanics/molecular mechanics (QM/MM) and full quantum mechanics calculations were carried out on the key catalytic steps, for "real-world" ligand systems, to clarify whether alkene coordination or hydride migration is the rate-determining step. Our calculations (21.4 kcal mol^{-1}) quantitatively reproduce the experimental energy barrier for CO dissociation (20.1 kcal mol^{-1}) starting at the (bisphosphane)$RhH(CO)_2$ resting state. The barrier for hydride migration lies 3.8 kcal mol^{-1} higher than the barrier for CO dissociation (experimentally determined trend ~3 kcal mol^{-1}). The computed $^{1}H/^{2}H$ and $^{12}C/^{13}C$ kinetic isotope effects corroborate the results of the energy analysis.

Keywords: density functional calculations · hydroformylation · isotope effects · phosphane ligands · reaction mechanisms

Introduction

The hydroformylation of alkenes is one of the most important homogeneously catalysed reactions in industry. The addition of carbon monoxide and hydrogen to alkenes, catalysed by homogeneous cobalt, rhodium or platinum catalysts, leads to the clean formation of aldehydes. The aldehydes are used in the manufacture of detergent and plasticiser alcohols and other butanal-derived products on a multi-ton scale. In principle, complete atom efficiency can be achieved; all atoms of the reactants are incorporated in the final product. This atom efficiency is crucial, because the production of these aldehydes exceeds eight million tons per annum.[1]

For the industrial production of butanal through hydroformylation of propene, several catalyst systems have been developed (and patented) that show high activity and high regioselectivity towards the formation of the desired linear aldehyde. These catalyst systems are based on rhodium, often modified by wide-bite-angle bidentate phosphane ligands based on the highly successful BISBI ligand backbone (BISBI = 2,2′-bis((diphenylphosphino)methyl)-1,1′-biphenyl), the Xanthene family of backbones[2] or related backbone structures.[3] Bulky wide-bite-angle diphosphite ligands have also been applied successfully in rhodium-catalysed hydroformylation reactions (see Scheme 1). These electron-poor ligands generate highly active catalyst systems that show very high regioselectivity towards the formation of linear aldehydes, even in the hydroformylation of internal alkenes to linear aldehydes.[4]

The generally accepted dissociative catalytic cycle for the hydroformylation of alkenes catalysed by phosphane-modified rhodium catalysts (Scheme 2) was first proposed by Wilkinson and co-workers.[5] Starting from trigonal-bipyramidal

[a] Dr. E. Zuidema, T. Eichelsheim, Prof. Dr. P. C. J. Kamer, Prof. Dr. P. W. N. M. van Leeuwen
Van't Hoff Institute for Molecular Sciences
Universiteit van Amsterdam, Nieuwe Achtergracht 166, 1018 WV Amsterdam, (The Netherlands)
E-mail: pwnm@science.uva.nl

[b] L. Escorihuela, Dr. J. J. Carbó, Dr. C. Bo
Universitat Rovira i Virgili, Campus Sescelades
Marcel.lí Domingo s/n, 43007 Tarragona (Spain)

[c] Dr. C. Bo, Prof. Dr. P. W. N. M. van Leeuwen
The Institute of Chemical Research of Catalonia
Avinguda Països Catalans 16, 43007 Tarragona (Spain)

Supporting information for this article is available on the WWW under http://www.chemeurj.org/ or from the author.

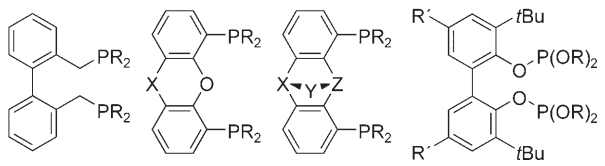

Scheme 1. Wide-bite-angle ligands applied in the rhodium-catalysed hydroformylation. From left to right: BISBI-based bidentate ligands, the xanthene family of ligands, diaryl bicyclo[2.2.*n*] compounds and wide-bite-angle diphosphite ligands.

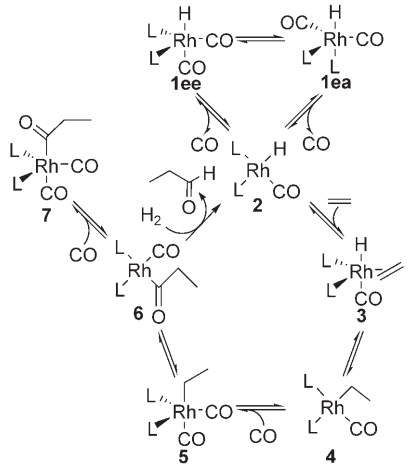

Scheme 2. Dissociative hydroformylation catalytic cycle as proposed by Wilkinson and co-workers.

rhodium hydride species **1**, coordinatively unsaturated species **2** is generated by loss of either one phosphane ligand or one carbon monoxide ligand. Alkene coordination yields 18-electron complex **3**, which can undergo hydride migration to form another coordinatively unsaturated species **4**. Carbon monoxide (re)coordination, followed by insertion yields acyl complex **6**. This complex can either react with carbon monoxide yielding complex **7** or it can react with H_2, liberating the aldehyde product and regenerating the rhodium hydride species **2**.

Under standard hydroformylation conditions, most reaction steps discussed above are believed to be reversible with the exception of the product-forming hydrogenolysis of species **6**. Furthermore, deuterioformylation experiments by Lazzaroni and co-workers by using the unmodified rhodium-carbonyl catalyst reveal that in the hydroformylation of both 1-hexene and styrene by using this catalyst system, the formation of alkyl complex **4** is essentially irreversible at room temperature. However, the formation of branched alkyl complexes becomes reversible at elevated temperatures.[6] Similar studies on the hydroformylation of 1-hexene by bisphosphane-modified rhodium catalysts by Casey and co-workers show that also for these electron-rich catalyst systems, the formation of alkyl complexes **4** is essentially irreversible under mild hydroformylation conditions.[7]

The relative rates of the individual reaction steps are influenced by the ligands employed in the reaction. Depending on the electronic and steric properties of the ligand, different reaction kinetics have been observed experimentally. Generally, the observed reaction kinetics are simplified to fit one of two extreme cases. For catalysts modified by electron-poor ligands such as bulky monophosphites and the unmodified rhodium-carbonyl catalyst, the hydrogenolysis of acyl species **6** controls the overall rate of hydroformylation.[8,9] Consequently, the observed rate of hydroformylation for these catalysts systems is independent of the alkene concentration, the rate shows a negative order in carbon monoxide concentration and it exhibits a first-order rate dependency on the hydrogen concentration (often referred to as Type II kinetics). The resting state of these catalysts is the acyl complex **7**, which has been observed spectroscopically.[8,10] In contrast, the kinetics for electron-rich ligands, including most bidentate phosphane ligands, are consistent with a rate-determining step early in the catalytic cycle (Type I kinetics). For these ligands the resting state of the catalyst is the penta-coordinate rhodium hydride species **1**. Previously, it has been shown that under the experimental conditions, the rate of carbon monoxide dissociation from complex **1** is two orders of magnitude higher than the overall rate of hydroformylation.[11,12] Therefore, either the rate of alkene coordination or the rate of hydride migration governs the overall rate of hydroformylation, but which one is actually rate-limiting remains unclear.

Here we present an investigation into the rate-determining step in the hydroformylation of 1-octene, catalysed by the rhodium–Xantphos catalyst system. In this study, we used a combination of $^{1}H/^{2}H$ and $^{12}C/^{13}C$ isotope effects to discriminate between alkene coordination and hydride migration as the rate-limiting step in the hydroformylation of 1-octene. The effect of isotopic substitution on the hydride moiety of the rhodium catalyst on the rate of hydroformylation was studied by comparing the relative rates of hydroformylation and deuterioformylation of 1-octene. Interestingly, whilst deuterioformylation has been used extensively to probe the reversibility of the formation of alkyl complex **4**, the relative rates of hydroformylation and deuterioformylation have not been compared previously. Since the addition of H_2 to complex **6** is not rate-limiting for these wide-bite-angle bisphosphane catalyst systems (Type I kinetics), the relative rates of hydroformylation and deuterioformylation should allow a direct discrimination between a rate-limiting alkene coordination and hydride migration reaction step in the hydroformylation of 1-alkenes. For the hydride migration reaction, which involves transfer of a hydride moiety from the metal centre to the coordinated alkene ligand, a large primary kinetic isotope effect would be expected. In contrast, the hydride moiety is not involved directly in the coordination of 1-octene to the metal centre. Therefore, if alkene coordination determines the overall rate of hydroformylation, the observed kinetic isotope effect would be expected to be small or absent.

To complement the $^{1}H/^{2}H$ kinetic isotope effect, $^{12}C/^{13}C$ kinetic isotope effects caused by the isotopic substitution in the alkene substrate were also investigated. If alkene coordi-

nation to complex **2** is rate-limiting, a primary kinetic isotope effect is expected at both the α-carbon and β-carbon positions of 1-octene, because both atoms are involved in the reaction similarly. On the other hand, if the hydride migration reaction is rate-determining, only one carbon atom is involved in the formation of the new carbon–hydrogen bond. The other carbon atom is involved in the formation of a rhodium–carbon σ-bond, but the vibrational energy of this bond is much lower than the vibrational energy of the carbon–hydrogen bond. Combined with the high kinetic preference for the formation of the linear aldehyde product for the Xantphos catalyst system, this would yield a large observed kinetic isotope effect at the β-position and a significantly smaller kinetic isotope effect at the α-position of the alkene substrate.

To explain the experimentally determined kinetic isotope effects and to unravel the rate-determining step of the reaction, DFT-based calculations on the initial steps of the hydroformylation reaction were performed on "real-world" rhodium–bisphosphane catalyst systems. Based on the combined experimental and the theoretical results, we were able to determine unambiguously the rate-limiting step in the hydroformylation of 1-octene, catalysed by the rhodium–Xantphos catalyst system.

Results and Discussion

^{1}H/^{2}H kinetic isotope effect: We have studied the relative rates of hydroformylation and deuterioformylation of 1-octene by using the rhodium–Xantphos catalyst system. The initial rate of aldehyde formation was determined by high-pressure infrared spectroscopy. Although this approach does not yield absolute rates of reaction, it does allow the comparison of different rates under identical reaction conditions. Furthermore, it allows us to study the initial rate of reaction in detail, revealing any incubation effects at the start of the reaction. Finally, the resting state of the catalyst can be monitored during the reaction. A change of the resting state of the catalyst from, for instance, complex **1** to acyl complex **7** might indicate a change in reaction kinetics between the hydroformylation and deuterioformylation of 1-octene.

Initially, the dependency of the rate of hydroformylation on the concentration of 1-octene in the reaction mixture was determined at 80 °C, at 20 bar of H_2/CO (1:1) and a rhodium concentration of 1.0 mM. The results are shown in Figure 1. A clear first-order rate dependence is observed, consistent with a rate-determining reaction step early in the catalytic cycle (Type I kinetics). Incubation effects after the addition of 1-octene were not observed. Subsequently, we studied the relative rates of hydroformylation and deuterioformylation at 80 °C and 20 bar of H_2/CO or D_2/CO at a rhodium concentration of 1.0 mM and an initial 1-octene concentration of 637 mM. An example of the graphs obtained from both the hydroformylation and deuterioformylation of 1-octene is shown in Figure 2. Clearly, for both hydroformylation and deuterioformylation, the reaction starts immediately and no incubation effects are observed. Although the formation of new carbon–deuterium bonds in the aldehyde product during deuterioformylation partially obscures the absorptions of the carbonyl ligands of the catalyst, no changes in the resting state were observed upon addition of alkene substrate, neither in the hydroformylation nor in the deuterioformylation reaction. The formation of acyl species **7**, which have a very characteristic infrared adsorption around 1675 cm^{-1} for phosphane-modified catalyst systems,[13] was not observed. Furthermore, GC analysis of the final products revealed no large differences between the regioselectivities of the hydroformylation and deuterioformylation reactions.

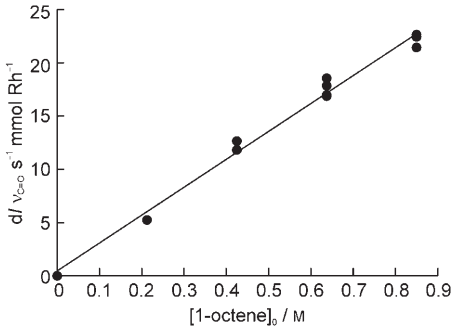

Figure 1. Dependence of the rate of hydroformylation (measured as the initial change in the intensity of the $\nu_{C=O}$ of the aldehyde product per second per mmol catalyst) on the initial 1-octene concentration[1-octene]$_0$, determined by high-pressure IR spectroscopy.

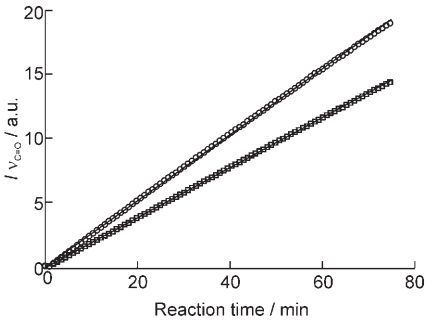

Figure 2. The rates of hydroformylation (○) and deuterioformylation (□) of 1-octene, monitored by the increase in the $\nu_{C=O}$ adsorption of the aldehyde product by high-pressure infrared spectroscopy.

The observed initial reaction rate for the hydroformylation of 1-octene was (17.6 ± 1.1) a.u. min^{-1} mmol Rh^{-1}, whereas the observed rate of deuterioformylation was (14.4 ± 1.8) a.u. min^{-1} mmol Rh^{-1}. This results in an observed kinetic ^{1}H/^{2}H isotope effect of 1.22 ± 0.11. These results were verified by regular batch autoclave experiments at 60 °C. The results from these experiments are shown in Table 1. From the turnover frequencies of hydroformylation and deuterioformylation, a ^{1}H/^{2}H kinetic isotope effect of 1.18 ± 0.02 was calculated, in good agreement with the experiments performed in the high-pressure infrared cell.

Table 1. Results of the hydro- and deuterioformylation of 1-octene.[a]

Experiment	TOF[b]	l/b	% Isomers[c]	% Nonanal[d]
H_2/CO	25.8±0.2	51±1	3±1	95±1
D_2/CO	21.8±0.4	54±2	3±1	95±1

[a] $T=60\,°C$, $pCO=pH_2=10$ bar, [Rh]=1.0 mM, Rh:L:1-octene=1:10:637. [b] Turnover frequency in (mol aldehyde)(mol rhodium)$^{-1}$ h^{-1}. [c] Percentage of octene isomers in all products formed in the reaction. [d] Percentage nonanal in all products formed in the reaction.

The observed kinetic isotope effect was small, suggesting a rate-limiting step for the hydroformylation of 1-octene which does not involve the transfer of the hydride moiety. However, the magnitude of the observed kinetic isotope effect greatly depends on the atoms involved in the reaction and the geometry of the transition state. Whilst for many organic reactions primary $^1H/^2H$ kinetic isotope effects of 5–7 are observed, many examples exist where the observed primary $^1H/^2H$ kinetic isotope effect is unusually small (or large).[14] Especially in reactions involving non-linear transition states, primary kinetic isotope effects can be much smaller than expected. Indeed, previous theoretical studies on the hydride migration step of the hydroformylation reaction have shown that the geometry of the transition state is far from linear.[15–20] Furthermore, because the hydride migration step in the hydroformylation reaction involves the breaking of a rhodium–hydride bond, which is significantly different from a carbon–hydrogen bond, interpretations purely based on a single small $^1H/^2H$ kinetic isotope effect can be misleading. A more detailed discussion is provided below.

$^{12}C/^{13}C$ kinetic isotope effects: $^{12}C/^{13}C$ isotope effects on the α-carbon and β-carbon atoms of 1-octene were determined at natural abundance by using the NMR methodology pioneered by Singleton and co-workers.[21] To this end, two samples of 1-octene were hydroformylated to high conversion (99.0% and 98.6%) at 60 °C and 20 bar of H_2/CO. The remaining octenes were subsequently recovered from the reaction mixture by column chromatography and distillation. The $^{12}C/^{13}C$ kinetic isotope effects were determined by quantitative $^{13}C\{^1H\}$ NMR spectroscopy by comparing the isotopic enrichment of the recovered samples against a commercial sample of 1-octene. The changes in isotopic composition of the α-carbon and β-carbon atoms in the recovered 1-octene relative to the commercial sample (R/R_0) were calculated by using the signal of the γ-carbon atom of 1-octene as an internal standard. The results are summarised in Table 2.

Within experimental error, the observed $^{12}C/^{13}C$ kinetic isotope effects on the α- and β-carbon atoms of 1-octene are identical. These results suggest a symmetrical transition state involving both α- and β-carbon atoms of 1-octene in the rate-limiting step of the hydroformylation reaction. Based on the high regioselectivity of the catalyst towards the formation of the linear aldehyde product (Table 1) and the irreversibility of the hydride migration step under the reaction conditions, there is a high kinetic preference for the hydride moiety to migrate to the β-carbon atom of the coordinated alkene ligand. Therefore, we would expect a large kinetic isotope effect on this carbon nucleus and a smaller kinetic isotope effect on the α-carbon nucleus of the alkene substrate if the migration step were rate-determining. This behavior was previously observed by Landis and co-workers in the polymerisation of 1-hexene by using zirconocene catalysts containing different counterions. The preferential 1,2-insertion of the coordinated 1-hexene moiety into the growing polymer chain resulted in the kinetic isotope effect at the β-carbon position of 1-hexene (1.02), which was larger than that observed at the α-carbon position (1.01) for all catalyst systems studied.

Table 2. Observed $^{12}C/^{13}C$ kinetic isotope effects on 1-octene.

Experiment	Conversion (%)	R/R_0		$^{12}C/^{13}C$ KIE	
		C_α	C_β	C_α	C_β
1	99.0	1.10(4)	1.08(3)	1.020(9)	1.016(6)
2	98.6	1.05(1)	1.053(5)	1.012(3)	1.012(1)

The observed $^{12}C/^{13}C$ kinetic isotope effects appear to be consistent with a rate-determining step involving the symmetrical addition of 1-octene to square-planar complex **2**. If alkene coordination to complex **2** proceeds through a symmetrical transition state, both the α-carbon and β-carbon atoms of the alkene are involved in the reaction similarly, leading to identical kinetic isotope effects on the two carbon nuclei. It should be noted that theoretical studies on the bimolecular alkene coordination step in the hydroformylation cycle are scarce in comparison to studies on the unimolecular hydride migration reaction.[19,20] As a consequence, little is known about the exact geometry of the transition state for this process. A recent computational study on ethene coordination to model rhodium complexes has suggested that the geometry of the transition state might be less symmetrical than expected.[20]

It should also be borne in mind that the kinetic isotope effects determined via this technique (i.e., at natural abundance) are heavily biased towards the rate-determining step at high substrate conversion. Because the rate of alkene addition is directly proportional to the alkene concentration, it is possible that 1-octene addition to complex **2** is not the slowest reaction step in the catalytic cycle at high substrate concentration, but that it becomes rate-determining as the concentration of 1-octene decreases during the reaction. Although both the determined $^1H/^2H$ and $^{12}C/^{13}C$ kinetic isotope effects seem to point towards a rate-determining step involving the symmetrical addition of 1-octene to complex **2**, a more detailed understanding of the transition states of the two reaction steps is required to unambiguously assign the rate-determining step in the rhodium–Xantphos-catalysed hydroformylation reaction.

Theoretical analysis of the key catalytic steps: To understand the observed kinetic isotope effects and unravel the rate-determining step in the hydroformylation reaction catalysed by rhodium catalysts modified by Xantphos-type ligands, we theoretically examined the early stages of the cat-

alytic cycle: i) CO dissociation; ii) alkene coordination, and; iii) hydride migration. To this end, hybrid quantum mechanics/molecular mechanics (QM/MM) and pure quantum mechanics (QM) calculations were carried out, for the "real-world" bisphosphane ligand and ethene as a model for alkenes. We focused our study on Thixantphos as a ligand (Scheme 3), which represents an intermediate case of natural bite angle among the series of Xantphos ligands, and for which the kinetic data for the CO dissociation and the overall reaction rates are available.[12]

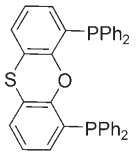

Scheme 3. The Thixantphos ligand.

First, we performed a systematic search of the possible isomers for species **1**, **2**, **3**, and the key transition states at QM/MM level. One of the main problems in theoretical characterisation of catalytic cycles is the growing number of coordination modes and ligand conformations to be considered. Although the Xantphos-type ligands are rather rigid, exhibiting pseudo-C_s symmetry, it is possible to define several ligand conformations and coordination modes (Figure 3). Two conformations of the non-planar Xanthene array of fused cycles were previously defined based on their bending about the central ring.[19] In the conformation designated *proximal* (**p**), this bending places the oxygen atom of the Xanthene ring closer to the rhodium than in the conformation designated *distal* (**d**). Additionally, we have also considered the possible rearrangements of phenyl moieties, taking the conformation of the crystal structure for (Nixantphos)Rh(CO)H(PPh_3)[12] for penta-coordinate species, and characterising several rotational conformations for tetracoordinated complex **2**. In penta-coordinate trigonal-bipyramidal complexes (e.g., **1** and **3**), the bisphosphane ligands can coordinate in an equatorial–equatorial (**ee**) or in an equatorial–axial (**ea**) manner. Assuming an axial preference of the hydride ligand and an equatorial coordination of the alkene,[16] it is possible to define two geometrical isomers for **ee** coordination by exchanging the relative positions of hydride and carbonyl axial ligands (**ee1** and **ee2**). Likewise, for **ea** alkene isomers the relative positions of ethene and equatorial carbonyl ligands leads to two different geometrical isomers, **ea1** and **ea2** (see Figure 3). In the case of the tetra-coordinate square-planar species **2**, the bisphosphane ligands can have a *cis* (**c**) or *trans* (**t**) rearrangement. A more detailed description of the geometries and relative energies of these isomers is provided in the Supporting Information. It is interesting to highlight some general qualitative trends. For a given species, the Thixantphos conformations lie within a relatively narrow interval of energies. In general, the *distal* isomers seem to be favoured over the *proximal*

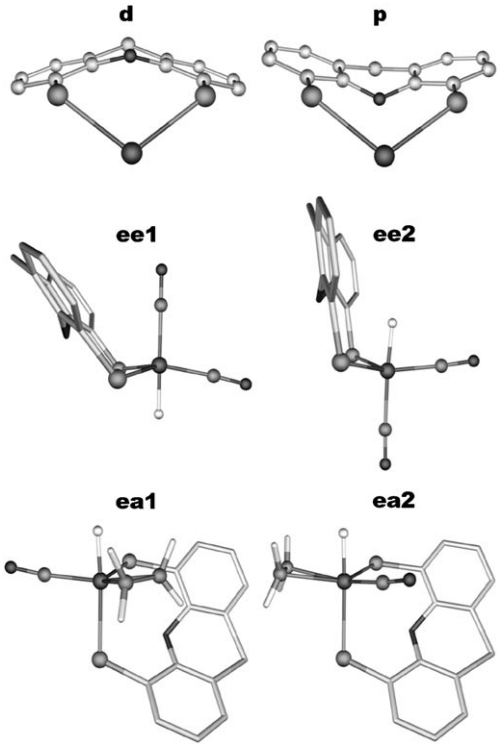

Figure 3. Different types of ligand conformers and complex isomers for species **1**, **2** and **3**. Thixantphos conformation *distal* (**d**) and *proximal* (**p**); and equatorial–equatorial (**ee**) and equatorial–axial (**ea**) geometrical ligand arrangements **ee1** and **ee2**, and **ea1** and **ea2**.

ones for penta-coordinate species, whereas for unsaturated tetra-coordinate species the situation with the oxygen of the Xanthene ring being closer to the rhodium seems more stable. The differences between lowest energy species for **ee** and **ea** isomers are less than 2 kcal mol^{-1}. In square-planar complexes **2**, the *cis* coordination mode of bisphosphane is lower in energy than the *trans* one by several kcal mol^{-1}. Finally, the **ee1** and **ea1** ligand rearrangement are more stable than their respective **ee2** and **ea2** geometrical isomers.

After this initial screening at the computationally affordable QM/MM level, we reoptimised the lowest energy isomers of equatorial–equatorial and equatorial–axial paths by means of full DFT calculations. Figure 4 summarises the calculated energetic profiles. The values correspond to electronic energies, which will be used for the discussion unless otherwise stated. The selection of Thixantphos ligand system allows us to compare our computed data directly with the previously reported experimental kinetic data. Making use of Transition State Theory one can estimate activation barriers from experimentally determined rate constants. The rate constant for CO dissociation in the [(Thixantphos)RhH($CO)_2$] complex derived from ^{13}CO exchange measurements in solution is about 200 h^{-1},[12] which leads to an estimated activation barrier of 20.1 kcal mol^{-1}. Moreover, based on experimental observations that the overall rate of the hydroformylation of 1-octene is estimated to be two orders of magnitude slower than the rate of CO dissocia-

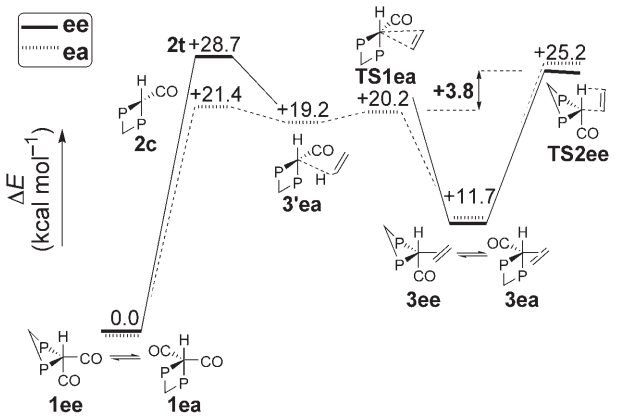

Figure 4. Potential energy profile (kcal mol^{-1}) for the early catalytic steps of the ethene hydroformylation catalysed by [(Thixantphos)RhH(CO)$_2$]. Relative energy values are computed at the full DFT level. Solid lines correspond to the equatorial–equatorial (**ee**) path, while dashed lines correspond to the equatorial–axial (**ea**) path.

tion,[12] the overall barrier of hydroformylation should be around 3 kcal mol^{-1} higher in energy than the barrier for CO dissociation. The initial dissociation of CO from the resting state [(Thixantphos)RhH(CO)$_2$] (**1**) was found to be barrierless.[19] Our computed values for this process are 28.7 and 21.4 kcal mol^{-1} for the **ee** and **ea** pathways, respectively (see Figure 4). The calculations reproduce experimental observations in that the dissociation of equatorial CO from the **ea** species is significantly faster than that from the **ee** complexes. Moreover, the calculated value for the **ea** pathway is in good agreement with the experimentally determined value.

The next step in the catalytic cycle consists of the coordination of the alkene substrate to form a penta-coordinate alkene complex **3**. The addition of ethene to **2t** and **2c** is predicted to be exothermic by 17.0 and 9.1 kcal mol^{-1}, respectively, leading to two isoenergetic ethene complexes **3ee** and **3ea**. Because the rate-determining step could be controlled by the reaction barriers from **2** to **3**, we examined this process in detail. Two theoretical studies on this step in the hydroformylation reaction have been reported previously. Gleich and co-workers have combined static and dynamic quantum-mechanical calculations to study alkene coordination in model phosphane complexes.[20] Their transition state searches only converged in the cases with apparently sufficient steric repulsion between the incoming substrate and the metal complex. They computed energy barriers ranging from −1.2 to +1.4 kcal mol^{-1}, increasing to the range from +8.3 to +10.2 kcal mol^{-1} after free energy corrections. For "real-world" Xantphos systems, Landis and co-workers have computed larger barriers at the QM/MM level, which span from +4.0 before to +17.1 kcal mol^{-1} after free energy corrections.[19]

Using full DFT calculations, we were unable to locate any transition state for ethene coordination through the bis-equatorial pathway. Even a relaxed scan of ethene approach to the tetra-coordinated *trans* complex **2t** did not yield a transition state, indicating that the process is barrierless (see Supporting Information for details). In contrast, a transition state (**TS1ea**) connecting the lowest energy isomers of the equatorial–axial path (**2c** and **3ea**) exists that is 1.2 kcal mol^{-1} lower in energy than complex **2c**. This means that at our computational level the equatorial–axial path is energetically favoured over the bis-equatorial one by at least 3.1 kcal mol^{-1}, which is the energy difference between *cis* and *trans* isomers of CO dissociation products. Nevertheless, the ethene coordination leads to an almost isoenergetic situation of the **3ee** and **3ea** ethene complexes, which then could easily interconvert via a Berry pseudorotation rearrangement with a small intrinsic barrier.[16] The negative activation barrier for ethene coordination through the **ea** path can be understood by the formation of a long-distance interaction η^1-(H) ethene intermediate (**3′**) that stabilises the unsaturated complex **2** by an energy of approximately 2 kcal mol^{-1} (see Figure 4). Introducing free energy contributions, the relative energy of **TS1ea** with respect to **2c** increases to +9.0 kcal mol^{-1}, which is a value similar to that from previous calculations. This increase of association energies in gas-phase calculations is due to the changing number of particles. In a more realistic system including solvent molecules, the entropic effects are expected to be smaller because of concomitant solvent reorganisation.[22] Thus, gas-phase Gibbs-free-energy calculations are expected to overestimate the entropy contributions of bimolecular processes such as ligand dissociation in solution. In fact, our computed Gibbs free energy for CO dissociation is 9.6 kcal mol^{-1}, which is significantly lower than the experimental value of 20.1 kcal mol^{-1}. Note that the latter experimental value is closer to that computed without entropic contributions (21.4 kcal mol^{-1}), suggesting that for calculations of bimolecular processes in vacuum the electronic energy differences are more reliable than the Gibbs-free-energy differences that do not take into account solvent rearrangement effects. Moreover, upon introduction of free-energy corrections, the energy difference between the resting state **1** and the **TS1ea** decreases from 20.2 to 18.6 kcal mol^{-1}. From this analysis of energetics, two main conclusions can be stated. First, the coordination of ethene to the catalyst species **2** is barrierless or occurs with a small energy barrier. Second, the energy required to reach the transition state for ethene coordination from the resting state of the catalyst **1** is lower than the energy required for carbonyl dissociation. Thus, the energy analysis suggests that the alkene coordination can be excluded as a candidate for the rate-determining step in the rhodium–Xantphos-catalysed hydroformylation of ethene.[23]

Finally, we have examined the hydride migration step. During this process, the alkene moiety rotates out of the equatorial plain of trigonal-bipyramidal complex **3** and subsequently, the hydride is transferred from the metal centre to the alkene moiety. The corresponding transition states **TS2ee** and **TS2ea** exhibited similar structural features to those in previous theoretical studies.[15,16,18–20,24] The barrier for the pathway originating from the **ee** ethene complex,

3ee→**TS2ee**, was computed to be 13.5 kcal mol^{-1}, whereas the barrier for the alternate pathway originating from the **ea** ethene complex, **3ea**→**TS2ea**, was computed to be 13.3 kcal mol^{-1}. In both cases, the calculated barriers are much lower than the estimated barrier for the overall reaction rate. If we consider the relative energy of the hydride migration transition state **TS2ee** with respect to the resting state **1ee**, the overall energy barrier of +25.2 kcal mol^{-1} becomes larger than the CO dissociation barrier. Interestingly, assuming a larger extent in error cancellation when we compare differences between activation barriers, the **TS2ee** structure is positioned 3.8 kcal mol^{-1} above that of the CO dissociation product **2c**, close to the estimated trend (3 kcal mol^{-1}) obtained from experimental data.[12] These results indicate that the energy barrier required for taking the catalyst from its resting state **1** to the transition state for hydride migration (**TS2**) controls the overall activity of catalytic cycle. Note that the direct comparison of the relative energies of the two transition states **TS1** and **TS2** is justified as both structures have the same number of atoms. Therefore the calculated free-energy corrections for the two structures will largely cancel. Furthermore, any negative entropy contributions in the alkene coordination step would lead to further destabilisation of alkene complex **3** and the subsequent hydride migration transition state **TS2** relative to the alkene coordination transition state **TS1**.

In fact, a closer inspection to the bibliography suggests that our findings are in line with previous theoretical studies on the full catalytic cycle employing model catalysts systems. Decker and Cundari,[18] and Morokuma and co-workers,[16] found that the transition state for hydride migration was the highest-energy species of the complete catalytic cycle. More recently, Gleich and Hutter[20] examined different model phosphane-modified catalysts, and observed that when free-energy corrections were considered, hydride migration was the highest energy point, whereas when no free-energy corrections were considered the CO dissociation product became the highest one, but only by 1–4 kcal mol^{-1} higher than the hydride migration TS.

In summary, the energy analysis points out that the process to reach the hydride migration TS from the resting state governs the overall activity in rhodium–Xantphos-catalysed hydroformylation of alkenes, in spite of the experimental kinetic isotope effects that seem to suggest a rate-determining step involving alkene coordination. To investigate the apparent contradiction between our theoretical analysis and the experimentally determined kinetic isotope effects and unambiguously determine the rate-limiting step in this process, we have also computed the kinetic isotope effects in the initial steps of the hydroformylation reaction.

Theoretical prediction of kinetic isotope effects: $^{1}H/^{2}H$ and $^{12}C/^{13}C$ kinetic isotope effects (KIEs) were investigated by using full DFT calculations on real-world ligand systems. Table 3 compares the experimentally observed KIEs with those computed from free-energy differences between the lowest ground state in energy **1ee** and the possible rate-determining transition states **TS1ea** and **TS2ee** for alkene coordination and hydride migration, respectively.

Table 3. Comparison of the experimentally observed $^{1}H/^{2}H$ and $^{12}C/^{13}C$ kinetic isotope effects (KIE) and the theoretical prediction for alkene coordination and hydride migration overall processes.

	$^{1}H/^{2}H$ KIE	$^{12}C/^{13}C$ KIE	
		C_α	C_β
experiment	1.22 ± 0.11	1.012(3)	1.012(1)
alkene coordination (**1ee**→**TS1ea**)	1.04	1.018	1.008
hydride migration (**1ee**→**TS2ee**)	1.52	1.010	1.015

As expected, our calculations predict a small secondary $^{1}H/^{2}H$ KIE of 1.04 for ethene coordination, whereas for hydride migration the value is slightly larger (1.52). Thus, the comparison of the computed values to the observed KIE (1.22) does not allow elimination of either of the two processes as the rate-determining step in the catalytic cycle. Considering the large $^{1}H/^{2}H$ KIE (5–7) observed for many proton-transfer organic reactions, the small $^{1}H/^{2}H$ KIE computed for the hydride migration process (1.52) may be surprising. However, one should consider some additional facts. First, the stretching frequencies of rhodium–hydride bonds are in the order of 2000 cm^{-1},[25] which is significantly lower than values of around 3000 cm^{-1} commonly observed for carbon–hydrogen bonds. For complex **1ee**, we calculate a value of 1987 cm^{-1}. By using the harmonic oscillator approximation, the corresponding rhodium-deuteride vibrational frequency was estimated to be 1424 cm^{-1}, in close agreement with previously reported Rh–D stretching frequencies calculated for model rhodium complexes.[12] From the calculated Rh–H and Rh–D stretching frequencies, a $^{1}H/^{2}H$ KIE of 3.4 is predicted at 60 °C for breaking the rhodium–hydride bond, which is considerably smaller than the $^{1}H/^{2}H$ KIE of 6.9 predicted for the breaking of a C–H bond. Secondly, the previous approximation is only valid if the Rh–H bond is broken at the transition state, which is not the case here. On going from **1ee** to **TS2ee**, the Rh–H bond lengthens by only 0.05 Å, indicating an early transition state containing a nearly unperturbed rhodium–hydride bond. For the transition state structure **TS2ee**, we identified a normal mode of vibration with a frequency of 1891 cm^{-1} corresponding to the rhodium-hydride stretching vibration. From this value, and by using the harmonic oscillator approximation, it is also possible to estimate a $^{1}H/^{2}H$ KIE associated with the partial bond breaking at the transition state of 1.1. This value is consistent with the computed $^{1}H/^{2}H$ KIE, which is smaller than that initially expected for hydride migration. Thus, we conclude that the small $^{1}H/^{2}H$ KIE observed experimentally for rhodium–Xantphos-catalysed hydroformylation of alkenes cannot preclude a rate-determining step involving hydride migration.

The nearly identical $^{12}C/^{13}C$-KIEs on the α-carbon and β-carbon atom of the terminal alkene observed experimentally suggest a symmetrical rate-determining transition state involving both carbon atoms. Closer inspection of the geometry of the transition state for ethene coordination **TS1ea** reveals that the incoming ethene ligand attacks the square-

planar complex **2c** perpendicularly relative to the H-Rh-P axis, with a H-Rh-C=C dihedral angle of −90.5°. More interestingly, one of the two approaching carbon atoms interacts more strongly with the rhodium centre than the other, resulting in two significantly different Rh−C distances of 3.106 and 3.400 Å. The carbon=carbon double bond slips over the carbonyl-rhodium-phosphane axis, forming a Rh-C-C attack angle of 90.9° (Figure 5). This asymmetric arrangement of

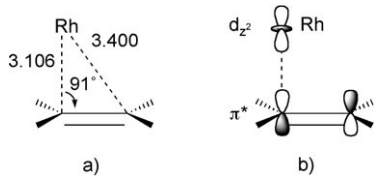

Figure 5. Schematic representation of the main geometrical parameters (a) and orbital interactions (b) in the transition state for alkene coordination **TS1ea**. Distances in Å and angles in deg.

the olefinic moiety at the transition state can be explained by considering that the rhodium centre reacts as a nucleophile attacking the empty π* orbital of the incoming alkene moiety. The Khon–Sham orbital energies calculated for the reactants **2**c and ethene agree with previous hypotheses.[26–28] The HOMO of the tetracoordinated d^8 rhodium complex is a Rh(d_{z^2})-based orbital, which is closer in energy to the empty ethene π* orbital than the ethene π orbital is to the empty Rh acceptor orbital. Thus, contrary to the classical description of the incoming ligand as the donor and the metal as acceptor of electron density, the mechanism for alkene coordination is best described as proceeding via nucleophilic attack of complex **2c** on the C=C bond of the alkene substrate. Moreover, the interaction of the HOMO on the metal and the LUMO on the ligand involves orbitals of different symmetry, and therefore the ethene has to slip to allow the interaction between the occupied Rh(d_{z^2}) and the empty π* orbitals, explaining the asymmetry of the transition state[26] (see Scheme 2). Analogous phenomena have been previously proposed in processes involving electron-rich transition-metal-based systems, such as, the alkene exchange at d^{10} palladium[28] and the addition of carbon monoxide to unsaturated tetra-coordinate d^8 Ir complexes.[27]

In accordance with geometrical parameters for **TS1ea**, the calculated $^{12}C/^{13}C$ KIE values for the closest carbon to rhodium (1.018) is larger than for the other carbon atom (1.008). Clearly, the use of the simplified ethene substrate does not allow us to distinguish between α- and β-carbon atoms. However, it is reasonable to assume that for a more realistic terminal alkene, the ligand attacks the complex preferably through one of the two olefinic carbons (α or β), and in the preferred transition state the alkene interaction with the metal is asymmetrical. It is known that the alkyl substituents polarise the π* orbital of the double bond towards the α-carbon atom,[29] exhibiting for propene larger DFT coefficients of the p-perpendicular atomic orbital in the non-substituted carbon atom. Thus, the nucleophilic interaction directs the attack of the rhodium lone pair in an orbital of d_{z^2} character to the α-carbon atom, which leads to a transition state with the α-carbon atom closer to the rhodium centre. Consequently, if alkene coordination were to determine the overall rate of hydroformylation, we would expect different carbon KIE values for both olefinic carbon atoms. Clearly, this is not in accordance with our experimental observations.

For hydride migration, on the other hand, the difference between the computed $^{12}C/^{13}C$ KIE of the two olefinic carbon atoms is smaller than for ethene coordination. Assuming that the whole reaction goes through the major prolinear path, the values for α- and β-carbon atoms are 1.010 and 1.015, respectively, which are in good agreement with the experimentally observed $^{12}C/^{13}C$ KIE values of 1.012(3) and 1.012(1), respectively. As we have already discussed, the transition state structure for hydride migration can be described as early with the rhodium−hydride bond only slightly perturbed with respect to the reactant. This indicates that most of the activation energy for hydride migration must be attributed to the rotation of the alkene from the equatorial in-plane arrangement in the reactant to a nearly perpendicular orientation in the transition state. Since this movement involves both olefinic carbons, similar $^{12}C/^{13}C$ KIE values are obtained for the α- and β-carbon atoms of the olefin, in agreement with experimental observations.

Conclusion

The rate-determining step in the hydroformylation of 1-octene, catalysed by the rhodium-Xantphos catalyst system, was determined by a combination of experimentally observed $^{1}H/^{2}H$ and $^{12}C/^{13}C$ kinetic isotope effects and a theoretical approach. Both the small $^{1}H/^{2}H$ kinetic isotope effect of 1.2 observed for the hydride moiety of the rhodium catalyst and the symmetrical $^{12}C/^{13}C$ kinetic isotope effects observed for the α- and β-carbon atoms of 1-octene suggest that addition of 1-octene to the square-planar complex **2** is the rate-limiting step in the hydroformylation of 1-octene catalysed by this catalyst system. Full DFT calculations on the catalytic cycle by using a "real-world" ligand system, however, suggest that the hydride migration is the rate-determining transition state. The calculations quantitatively reproduce the experimentally determined energy barrier for carbonyl dissociation in the Thixantphos ligand system (20.1 kcal mol^{-1} experimentally versus 21.4 kcal mol^{-1} theoretically). The individual barriers for the other two elementary steps of the catalytic cycle are consistent with Type I kinetics, that is, alkene coordination and hydride migration show significantly lower values (1 and 13 kcal mol^{-1}, respectively). If one considers the energy differences between the lowest ground state in energy, the resting state **1**, and the transition states for alkene coordination and hydride migration, the barriers increase to values close to that determined for carbonyl dissociation.

Moreover, whilst the overall barrier for alkene coordination is lower than that for CO dissociation, the energy requirement to undergo hydride migration from the resting state of the catalyst is 3.8 kcal mol^{-1} higher than the barrier for CO dissociation, which is in good agreement with the trend estimated from previous experimental data.

Computed $^{1}H/^{2}H$ and $^{12}C/^{13}C$ KIE values support the conclusions drawn from the energy analysis of the initial steps in the catalytic cycle and also explain the experimentally determined kinetic isotope effects. Due to the "early nature" of the TS for hydride migration, containing a nearly unperturbed rhodium–hydride bond, the computed $^{1}H/^{2}H$ KIE values are smaller than expected, and therefore, the small $^{1}H/^{2}H$ KIE values observed experimentally cannot preclude a rate-determining step involving hydride migration. On the other hand, the asymmetric nature of the transition state for alkene coordination leads to non-symmetric $^{12}C/^{13}C$ KIE values for the α-carbon and β-carbon atoms of the alkene substrate, which are not in accordance with our experimentally determined values. The combined experimental and theoretical results strongly suggest that the overall process from the pentacoordinated rhodium hydride resting state species **1** to hydride migration **3**→**4** governs the overall activity in the rhodium-Xantphos-catalysed hydroformylation of 1-octene. In this context, the term "rate-determining step" can be misleading because it implies that a single slow step in the catalytic cycle is responsible for the overall rate of reaction. Although the overall rate of hydroformylation is limited by the rate of hydride migration, both CO dissociation and alkene coordination contribute to the overall barrier. Therefore it is more accurate to say that the rate of hydroformylation is determined by a set of reactions ending in hydride migration. Finally, we would like to note that during revision of the manuscript Sparta and co-workers have published a theoretical study on the activity of rhodium-catalyzed hydroformylation leading to the same conclusion as us for catalysts modified by electron-donating ligands.[30]

Experimental Section

Standard syringe techniques were applied for transfer of air-sensitive reagents and dry solvents. Commercially available chemicals were used without further purification, unless stated otherwise. Cyclohexane was purchased from Rathburn, distilled from over sodium wire and stored under argon. Toluene was purchased from Rathburn and distilled from over sodium pieces. Pentane was purchased from Biosolv and distilled from solution containing sodium/benzophenone/triglyme. 1-Octene was purchased from Sigma–Aldrich and was purified over neutral aluminium oxide prior to use. Nonanal was purchased from Sigma–Aldrich. Aluminum oxide, 90 active neutral (0.063–0.2 mm), was purchased from Merck. Silica gel 100 (0.2–0.5 mm) was purchased from Biosolv. Naphthalene was purchased from Acros chemical company and [Rh(acac)(CO)$_2$] was purchased from Merck. Xantphos was synthesised according to a literature procedure.[31] NMR spectra were recorded on a Varian Inova 500 MHz spectrometer.

Computational details: Full quantum mechanics calculations on the Thixantphos ligand system were performed with the GAUSSIAN 98 series of programs[32] within the framework of the density functional theory (DFT)[33] using the B3LYP functional.[34] A quasi-relativistic effective core potential operator was used to represent the 28 innermost electrons of the Rh atom, as well as the 10 innermost electrons of the P and S atoms.[35] The basis set for Rh, P and S atoms was that associated with the pseudopotential,[35] with a standard double-ξ LANL2DZ contraction,[32] and in the case of P was supplemented by a d shell.[36] The 6-31G(d) basis set was used for the alkene carbons and the carbonyl ligand,[37] the 6-31G(p) basis set was used for the hydride ligand and alkene hydrogen atoms,[37] whereas the 6-31G basis set was used for the other atoms.[37] Geometry optimisations were carried out without any symmetry restrictions and all stationary points were optimised with analytical first derivatives. Transition states were characterised by single imaginary frequency, the normal mode of which corresponded to the expected motion. Kinetic isotope effects were calculated by using statistical mechanics employing harmonic vibrational frequencies obtained from frequency calculations.[32] The initial energy analysis of the possible isomers (see Supporting Information) was performed by means of the more computationally affordable hybrid quantum mechanics/molecular mechanics (QM/MM) calculations, by using the ONIOM method[38] as implemented in the GAUSSIAN 98 series of programs.[32] The QM region of the catalysts was [RhH(CO)(PH$_3$)$_2$], whereas the substrate ethene was fully in the QM region. The QM level was the same as described above. Molecular mechanics calculations used the UFF force field.[39]

Hydroformylation and deuterioformylation using high-pressure infrared spectroscopy: The high-pressure infrared (HP-IR) spectroscopic experiments were preformed in a stainless-steel (SS 316) 50-mL autoclave equipped with IRTRAN windows (ZnS, transparent up to 700 cm^{-1}, 10 mm id, optical path length = 0.4 mm), a mechanical stirrer, a temperature controller, a pressure transducer and a separate 50-mL second chamber. In a typical experiment the IR autoclave was filled with a solution of [Rh(acac)(CO)$_2$] (4 mg, 15 μmol) and Xantphos (93 mg, 160 μmol) in cyclohexane (10.0 mL), prepared under an inert atmosphere. The autoclave was purged three times with a 1:1 mixture of H/CO or D$_2$/CO (22 bar) and was subsequently pressurised to 17 bar. The second chamber was filled with a solution (5 mL) of 1-octene (0.5 mL, 1.0 mL, 1.5 mL and 2.0 mL) and decane (0.75 mL, 3.88 mmol) in cyclohexane. This chamber was flushed three times with H$_2$/CO or D$_2$/CO (22 bar) and was subsequently pressurised to 22 bar. The autoclave was heated to 80 °C and was allowed to stabilise for 1 h. Rapid-scan IR measurements were started (120 min, 4 scans per spectrum, 10 s between spectra, resolution 2 cm^{-1}) immediately followed by the addition of the 1-octene solution to the catalyst solution. Difference spectra were obtained by subtraction of the infrared spectrum taken after 1.077 minutes from the other spectra. The increase in peak area of the nonanal aldehyde signal (area 1674–1811 cm^{-1}) over time was analysed by linear regression.

Hydroformylation and deuterioformylation of 1-octene: The hydroformylation experiments were performed in a stainless-steel (SS 316) autoclave (196 mL). The autoclave was stirred mechanically and was equipped with a separate reservoir, a pressure transducer and a thermocouple. In a typical experiment [Rh(acac)(CO)$_2$] (5.2 mg, 20 μmol) and Xantphos (120 mg, 0.2 mmol) were dissolved in toluene (15.0 mL) under inert atmosphere. The autoclave was placed under vacuum for 30 min and was subsequently purged three times using H$_2$/CO or D$_2$/CO (15 bar). The catalyst solution was introduced into the autoclave by using a syringe. The autoclave was purged an additional three times and was subsequently pressurised to 15 bar and heated to 60 °C. The solution was stirred at this temperature for 1 h. A mixture of 1-octene (2 mL, 12.74 mmol), decane (internal standard, 1.0 mL, 5.17 mmol) and toluene (2 mL) was introduced into the separate reservoir and the reservoir was purged three times using H$_2$/CO or D$_2$/CO (20.0 bar). The substrate solution was introduced into the autoclave by overpressure and the autoclave was pressurised to a total pressure of 20.0 bar. The hydroformylation reaction was stopped after a pressure drop of approximately 0.5 bar by using a solution of tributylphosphite. The autoclave was cooled rapidly by using an ice-water bath and was depressurised. The conversion and product distribution were determined by GC analysis of the reaction mixture.

$^{12}C/^{13}C$ Kinetic isotope effect: Hydroformylation of 1-octene: Hydroformylation experiments were performed in a stainless-steel (SS 316) autoclave (196 mL). The autoclave was equipped with a mechanical stirrer

and was also equipped with a separate reservoir, a pressure transducer and a thermocouple. In a typical experiment, $[Rh(acac)(CO)_2]$ (5.2 mg, 20 μmol) and Xantphos (120 mg, 210 μmol, 10 equiv) were placed in the autoclave. The autoclave was closed, evacuated for 30 min and was subsequently purged by using a mixture of H_2/CO (1:1, 20 bar). Naphthalene (0.5 g, 3.9 mmol) was dissolved in purified 1-octene (20 mL, 127 mmol) under inert atmosphere and this mixture was subsequently introduced into the autoclave. The autoclave was purged three times with a mixture of H_2/CO (1:1, 20 bar) and pressurised to 20 bar. The reaction mixture was heated to 60 °C. At regular intervals the autoclave was repressurised to 20 bar. The pressure was not allowed to decrease below 18 bar. The reaction was run to high conversion and was stopped by rapidly cooling the autoclave in an ice/water bath, followed by depressurisation. After opening the autoclave, the reaction mixture was collected and stored under argon. Conversions were determined by gas chromatography.

Recovery of octenes from hydroformylation reaction mixtures: The remaining alkenes in the hydroformylation reaction mixture were isolated by column chromatography over silica, using pentane as an eluent. The collected fractions were analysed by gas chromatography. Fractions containing 1-octene were combined and concentrated to 2–3 mL by fractional distillation of the solvent. GC analysis showed no significant amounts of octenes in the distilled solvent. To remove trace amounts of pentane still present in the residue, dry $CDCl_3$ (10 mL) was added to the mixture and the resulting solution was concentrated a second time to 2–3 mL by careful distillation. For comparison, a commercial sample of 1-octene (0.3 mL, 1.9 mmol) in nonanal (5 mL) was subjected to the same purification procedure.

Determination of the $^{12}C/^{13}C$ kinetic isotope effect: Both the commercial sample and the recovered octene mixtures were analysed by quantitative $^{13}C\{^1H\}$ NMR spectroscopy. NMR samples were prepared under argon, placing 1.5 mL of the octene solution in a 5 mm NMR-tube. $^{13}C\{^1H\}$ NMR spectra were collected at 125.69 MHz, by using inverse-gated-decoupling in order to minimise nuclear Overhauser effects. A spectral width of 200.00 ppm was used. The T_1 relaxation times were determined for all samples using the inversion-recovery method. Based on these measurements, a recycle delay of 108 s (at least $6 \times T_1$) between calibrated $\pi/2$ pulses was chosen. An acquisition time of 7.00 s was used, collecting 175935 points. Integrations were determined by using a constant region of ± 5 times the peak-width-at-half-height. A zero-order baseline correction was applied, but in no case was a first-order correction applied. A total of four spectra were obtained for each sample.

Acknowledgements

This work was supported by the Netherlands Organisation for Scientific Research (NWO/CW). The authors are grateful for financial support from the MEC of Spain (CTQ2005-06909-C02-02/BQU, CTQ2005-06909-C02-01/BQU and Consolider Ingenio 2010 CSD2006-0003), from the Generalitat de Catalunya (2005SGR00715 and 2005SGR00104), and from the ICIQ Foundation. The SARA Centre For High Performance Computing is acknowledged for use of their computational facilities.

[1] C. D. Frohning, C. W. Kohlpainter in *Applied Homogeneous Catalysis with Organometallic Compounds, Vol. 1* (Eds.: B. Cornils, W. A. Herrman), VCH Publishers, New York, NY (USA), **1996**.

[2] a) H. Bohnen, J. Herwig, A. Joerg, D. Hoff, S. Surm, P. W. N. M. van Leeuwen, R. Bronger, O. Stelzer (Celanese Chemicals Europe GmbH), DE 10225282, **2003**; b) H. Bohnen, J. Herwig (Celanese Chemicals Europe GmbH), WO 2002068371, **2002**; c) H. Bohnen, J. Herwig (Celanese Chemicals Europe GmbH, Germany), WO 2002068369, **2002**; d) W. Ahlers, R. Paciello, D. Vogt, P. Hofmann (BASF Aktiengesellschaft), WO 2002083695, **2002**; e) W. Ahlers, D. Wiebelhaus, R. Paciello, M. Bartsch, R. Baumann, D. Vogt, A. Hewat (BASF Aktiengesellschaft), WO 2002022261, **2002**; f) P. Rainer, W. Ahlers, T. Mackewitz, R. Paciello, M. Volland (BASF Aktiengesellschaft), WO 2005039762, **2005**; g) P. W. N. M. van Leeuwen, E. B. Walczuk-Gusciora, N. E. Grimmer, P. C. J. Kamer (Sasol Technology Proprietary Limited), WO 2005049537, **2005**.

[3] W. Ahlers, M. Roeper, P. Hofmann, D. C. M. Warth, R. Paciello (BASF Aktiengesellschaft), WO 2001058589, **2001**.

[4] a) E. Billig, A. G. Abatjoglou, D. R. Bryant, R. E. Murray, J. M. Maher (Union Carbide Corp.), US pat. 4,599,206, **1986**; b) E. Billig, A. G. Abatjoglou, D. R. Bryant (Union Carbide Corp.), US Pat. 4,668,651; US Pat. 4748261, **1987**.

[5] D. Evans, J. A. Osborn, G. Wilkinson, *J. Chem. Soc. A* **1968**, 3133.

[6] a) R. Lazzaroni, G. Uccello-Barretta, M. Benetti, *Organometallics* **1989**, *8*, 2323; b) G. Uccello-Barretta, R. Lazzaroni, R. Settambolo, P. Salvadori, *J. Organomet. Chem.* **1991**, *417*, 111; c) A. Raffaelli, S. Pucci, R. Settambolo, G. Uccello-Barretta, R. Lazzaroni, *Organometallics* **1991**, *10*, 3892.

[7] C. P. Casey, L. M. Petrovich, *J. Am. Chem. Soc.* **1995**, *117*, 6007.

[8] M. Garland, P. Pino, *Organometallics* **1991**, *10*, 1693.

[9] a) V. S. Nair, S. P. Mathew, R. V. Chaudhari, *J. Organomet. Chem.* **1999**, *143*, 99; b) J. Feng, M. Garland, *Organometallics* **1999**, *18*, 417.

[10] P. C. J. Kamer, A. Van Rooy, G. C. Schoemaker, P. W. N. M. Van Leeuwen, *Coord. Chem. Rev.* **2004**, *248*, 2409.

[11] a) L. A. van der Veen, P. C. J. Kamer, P. W. N. M. Van Leeuwen, *Organometallics* **1999**, *18*, 4765; b) L. A. van der Veen, P. C. J. Kamer, P. W. N. M. Van Leeuwen, *Angew. Chem.* **1999**, *111*, 349; *Angew. Chem. Int. Ed.* **1999**, *38*, 336.

[12] L. A. van der Veen, P. H. Keeven, G. C. Schoemaker, J. N. H. Reek, P. C. J. Kamer, P. W. N. M. Van Leeuwen, M. Lutz, A. L. Spek, *Organometallics* **2000**, *19*, 872.

[13] a) G. Yagupski, C. K. Brown, G. Wilkinson, *Chem. Commun.* **1969**, 1244; b) J. Zhang, M. Poliakoff, M. W. George, *Organometallics* **2003**, *22*, 1612; c) M. Caporali, P. Frediani, A. Salvini, G. Laurenczy, *Inorg. Chim. Acta* **2004**, *357*, 4537.

[14] F. H. Westheimer, *Chem. Rev.* **1961**, *61*, 265.

[15] a) N. Koga, S. Q. Jin, K. Morokuma, *J. Am. Chem. Soc.* **1988**, *110*, 3417; b) D. G. Musaev, T. Matsubara, A. M. Mebel, N. Koga, K. Morokuma, *Pure Appl. Chem.* **1995**, *67*, 257; c) W. R. Rocha, W. B. D. Almeida, *Int. J. Quantum Chem.* **2000**, *78*, 42; d) G. Alagona, C. Ghio, R. Lazzaroni, R. Settambolo, *Organometallics* **2001**, *20*, 5394; e) R. Schmid, W. A. Herrmann, G. Frenking, *Organometallics* **1997**, *16*, 701; f) D. Gleich, R. Schmid, W. A. Herrmann, *Organometallics* **1998**, *17*, 4828; g) D. Gleich, R. Schmid, W. A. Herrmann, *Organometallics* **1998**, *17*, 2141; h) D. Gleich, W. A. Herrmann, *Organometallics* **1999**, *18*, 4354; i) J. J. Carbo, F. Maseras, C. Bo, P. W. N. M. van Leeuwen, *J. Am. Chem. Soc.* **2001**, *123*, 7630; j) J. J. Carbó, A. Lledós, D. Vogt, C. Bo, *Chem. Eur. J.* **2006**, *12*, 1457; k) E. Zuidema, E. Daura-Oller, J. J. Carbó, C. Bo, P. W. N. M. van Leeuwen, *Organometallics* **2007**, *26*, 2234.

[16] T. Matsubara, N. Koga, Y. Ding, D. G. Musaev, K. Morokuma, *Organometallics* **1997**, *16*, 1065.

[17] S. A. Decker, T. R. Cundari, *J. Organomet. Chem.* **2001**, *635*, 132.

[18] S. A. Decker, T. R. Cundari, *New J. Chem.* **2002**, *26*, 129.

[19] C. R. Landis, J. Uddin, *J. Chem. Soc. Dalton Trans.* **2002**, 729.

[20] D. Gleich, J. Hutter, *Chem. Eur. J.* **2004**, *10*, 2435.

[21] D. A. Singleton, A. A. Thomas, *J. Am. Chem. Soc.* **1995**, *117*, 9357.

[22] S. F. Vyboishchikov, M. Bühl, W. Thiel, *Chem. Eur. J.* **2002**, *8*, 3962.

[23] In the calculations, ethene was chosen as a model substrate to decrease the number of structural isomers caused by the distinct orientations of the alkene moiety in the metal complexes. For real-life 1-octene, steric repulsion might destabilise transition state **TS1**, resulting in comparable transition state energies for CO dissociation and alkene coordination.

[24] S. A. Decker, T. R. Cundari, *Organometallics* **2001**, *20*, 2827.

[25] a) A. R. Sanger, *J. Mol. Cat.* **1977**, *3*, 221; b) A. R. Sanger, L. R. Schallig, *J. Mol. Cat.* **1977**, *3*, 101.

[26] a) O. Eisenstein, R. Hoffmann, *J. Am. Chem. Soc.* **1980**, *102*, 6148; b) O. Eisenstein, R. Hoffmann, *J. Am. Chem. Soc.* **1981**, *103*, 4308.

[27] F. Abu-Hasanayn, K. Krogh-Jespersen, A. S. Goldman, *J. Am. Chem. Soc.* **1994**, *116*, 5979.

[28] B. V. Popp, J. L. Thorman, C. M. Morales, C. R. Landis, S. S. Stahl, *J. Am. Chem. Soc.* **2004**, *126*, 14832.

[29] a) K. N. Houk, J. Sims, R. E. Duke, Jr., R. W. Strozier, J. K. George, *J. Am. Chem. Soc.* **1973**, *95*, 7287; b) D. P. Fox, P. J. Stang, Y. Apeloig, M. Karni, *J. Am. Chem. Soc.* **1986**, *108*, 750.
[30] M. Sparta, J. Børve, V. R. Jensen, *J. Am. Chem. Soc.* **2007**, *129*, 8487.
[31] M. Kranenburg, Y. E. M. van der Burgt, P. C. J. Kamer, P. W. N. M. Van Leeuwen, K. Goubitz, J. Fraanje, *Organometallics* **1995**, *14*, 3081.
[32] M. J. Frisch, G. W. Trucks, H. B. Schlegel, G. E. Scuseria, M. A. Robb, J. R. Cheeseman, V. G. Zakrzewski, J. J. A. Montgomery, R. E. Stratmann, J. C. Burant, S. Dapprich, J. M. Millam, A. D. Daniels, K. N. Kudin, M. C. Strain, O. Farkas, J. Tomasi, V. Barone, M. Cossi, R. Cammi, B. Mennucci, C. Pomelli, C. Adamo, S. Clifford, J. Ochterski, G. A. Petersson, P. Y. Ayala, Q. Cui, K. Morokuma, D. K. Malick, A. D. Rabuck, K. Raghavachari, J. B. Foresman, J. Cioslowski, J. V. Ortiz, A. G. Baboul, B. B. Stefanov, G. Liu, A. Liashenko, P. Piskorz, I. Komaromi, R. Gomperts, R. L. Martin, D. J. Fox, T. Keith, M. A. Al-Laham, C. Y. Peng, A. Nanayakkara, C. Gonzalez, M. Challacombe, P. M. W. Gill, B. G. Johnson, W. Chen, M. W. Wong, J. L. Andres, M. Head-Gordon, E. S. Replogle, J. A. Pople, Gaussian 98 (Revision A.7), Gaussian Inc., Pittsburg, PA, **1998**.
[33] a) R. G. Parr, W. Yang, *Density Functional Theory of Atoms and Molecules*, Oxford University Press, Oxford (UK), **1989**, p. 352; b) T. Ziegler, *Chem. Rev.* **1991**, *91*, 651.
[34] a) C. Lee, W. Yang, R. G. Parr, *Phys. Rev. B* **1988**, *37*, 785; b) A. D. Becke, *J. Chem. Phys.* **1993**, *98*, 5648; c) P. J. Stephens, F. J. Devlin, C. F. Chabalowski, M. J. Frisch, *J. Phys. Chem.* **1994**, *98*, 11623.
[35] P. J. Hay, W. R. Wadt, *J. Chem. Phys.* **1985**, *82*, 299.
[36] A. Höllwarth, M. Böhme, S. Dapprich, A. W. Ehlers, A. Gobbi, V. Jonas, K. F. Köhler, R. Stegmann, A. Veldkamp, G. Frenking, *Chem. Phys. Lett.* **1993**, *208*, 237.
[37] a) M. M. Francl, W. J. Pietro, W. J. Hehre, J. S. Binkley, M. S. Gordon, D. J. Defrees, J. A. Pople, *J. Chem. Phys.* **1982**, *77*, 3654; b) W. J. Hehre, R. Ditchfield, J. A. Pople, *J. Chem. Phys.* **1972**, *56*, 2257; c) P. C. Hariharan, J. A. Pople, *Theor. Chim. Acta* **1973**, *28*, 213.
[38] a) F. Maseras, K. Morokuma, *J. Comput. Chem.* **1995**, *16*, 1170; b) F. Maseras, *Chem. Commun.* **2000**, 1821; c) S. Humbel, S. Sieber, K. Morokuma, *J. Chem. Phys.* **1996**, *105*, 1959; d) M. Svensson, S. Humbel, R. D. J. Froese, T. Matsubara, S. Sieber, K. Morokuma, *J. Phys. Chem.* **1996**, *100*, 19357; e) M. Svensson, S. Humbel, K. Morokuma, *J. Chem. Phys.* **1996**, *105*, 3654; f) S. Dapprich, I. Komáromi, K. S. Byun, K. Morokuma, M. J. Frisch, *J. Mol. Struct.* **1999**, *462*, 1.
[39] A. K. Rappé, C. J. Casewit, K. S. Colwell, W. A. Goddard III, W. M. Skiff, *J. Am. Chem. Soc.* **1992**, *114*, 10024.

Received: May 12, 2007
Revised: October 22, 2007
Published online: December 5, 2007

